Orthogonal Contrastive Learning for Multi-Representation fMRI Analysis

Tony Muhammad Yousefnezhad[1,2,*]
[1]Learning By Machine
[2]Information Management, National Bank of Canada
Edmonton AB Canada
tony@learningbymachine.com

Abstract

Task-based functional magnetic resonance imaging (fMRI) provides invaluable insights into human cognition but faces critical hurdles—low signal-to-noise ratio, high dimensionality, limited sample sizes, and costly data acquisition—that are amplified when integrating datasets across subjects or sites. This paper introduces orthogonal contrastive learning (OCL), a unified multi-representation framework for multi-subject fMRI analysis that aligns neural responses without requiring temporal preprocessing or uniform time-series lengths across subjects or sites. OCL employs two identical encoders: an online network trained with a contrastive loss that pulls together same-stimulus responses and pushes apart different-stimulus responses, and a target network whose weights track the online network via exponential moving average to stabilize learning. Each OCL network layer combines QR decomposition for orthogonal feature extraction, locality-sensitive hashing (LSH) to produce compact subject-specific signatures, positional encoding to embed temporal structure alongside spatial features, and a transformer encoder to generate discriminative, stimulus-aligned embeddings. We further enhance OCL with an unsupervised pretraining stage on fMRI-like synthetic data and demonstrate a transfer-learning workflow for multi-site studies. Across extensive experiments on multi-subject and multi-site fMRI benchmarks, OCL consistently outperforms state-of-the-art alignment and analysis methods in both representation quality and downstream classification accuracy.

1 Introduction

Task-based functional magnetic resonance imaging (fMRI) is a widely used technique in neuroscience for studying brain activity during cognitive processes such as decision-making, perception, and attention [1, 2, 3, 4]. By capturing blood-oxygen-level-dependent (BOLD) signals while subjects engage in structured tasks, fMRI enables researchers to link brain regions to specific mental functions [5]. Despite its potential, fMRI data present several challenges: they are high-dimensional, inherently noisy, expensive to acquire, and often limited in sample size—factors that hinder the training and generalization of machine learning models [1, 2, 3, 4, 6, 7]. To mitigate these limitations, modern research increasingly relies on multi-subject fMRI datasets to improve model robustness and validity. Moreover, the growing availability of large-scale, open-access repositories such as the national

[*] This research study is conducted independently and is not connected to the author's role at the *National Bank of Canada.*

39th Conference on Neural Information Processing Systems (NeurIPS 2025).

institute of mental health (NIMH) [2], the Human Connectome Project [3], and OpenNEURO [4] has made it feasible to aggregate homogeneous task-based fMRI data across multiple sites, thereby increasing sample diversity and statistical power [1, 7]. However, this introduces additional complexity, including inter-subject variability, cross-site differences in scanner hardware and acquisition protocols, and population-level heterogeneity [1, 7, 8]. Consequently, there is a pressing need for machine learning frameworks that can generalize across sites and subjects while being resilient to such batch effects, making the development of domain-adaptive, multi-representation learning techniques essential for real-world fMRI analysis.

Multi-subject fMRI analysis is complicated by substantial inter-individual variability in brain connectivity, as each person's connectome exhibits unique structural and functional patterns that lead to idiosyncratic neural responses across subjects [2, 9]. To address this, functional alignment techniques—most notably hyperalignment [5] and shared response model (SRM) [6, 10]—project each subject's neural responses into a shared representational space using an orthogonal mapping procedure, effectively realigning neural signatures and improving inter-subject correspondence. These alignment strategies can be framed as multi-view learning problems—each subject constitutes a 'view', and methods like generalized canonical correlation analysis (CCA) identify transformations that maximize shared information across views [2, 6, 9, 10, 11, 12, 13]. Recent work has extended functional alignment to multi-site fMRI studies, aiming to pool data from different scanners and populations; however, these efforts must contend with batch effects arising from scanner hardware differences, acquisition protocols, and site-specific demographics [1, 7, 8]. Such batch effects introduce unwanted variability that can confound downstream analyses unless corrected by harmonization methods such as domain-adaptation frameworks tailored to neuroimaging [1, 7]. Constructive learning [14, 15, 16, 17, 18, 19, 20] is a paradigm in which models learn by contrasting similar and dissimilar example pairs to shape feature spaces. It complements multi-view functional alignment by using contrastive objectives to directly align representations across subjects and sites and, by enforcing agreement on same-stimulus responses while discouraging spurious correlations, helps mitigate batch effects and enhances robustness and generalization in multi-site fMRI analyses.

The main contributions of this paper are fivefold: (1) we introduce orthogonal contrastive learning (OCL), a unified multi-representation framework that aligns multi-subject fMRI data without temporal preprocessing or uniform time-series length requirements across subjects or sites; (2) we design a dual-encoder architecture—an online network trained with a contrastive loss that pulls same-stimulus responses together and pushes different-stimulus responses apart, and a target network updated via exponential moving average to stabilize learning and enforce consistency; (3) we develop a novel OCL layer composed of four tightly integrated components: QR decomposition, which yields orthonormal feature bases to decorrelate signals and enhance the signal-to-noise ratio; locality-sensitive hashing (LSH) [21], which produces compact subject-specific signatures that preserve similarity relationships while drastically reducing feature dimensionality; positional encoding, which injects continuous temporal context into spatial feature representations to maintain dynamic stimulus information; and a transformer encoder, which employs multi-head self-attention to capture global dependencies and produce discriminative, stimulus-aligned embeddings; (4) we propose an unsupervised pretraining strategy on synthetic fMRI-like data to initialize OCL parameters for faster convergence and improved robustness; and (5) we demonstrate a transfer-learning pipeline that applies trained OCL models to multi-site datasets, showing resilience to scanner variability and sequence-length differences, and achieving superior downstream classification performance over state-of-the-art methods.

The remainder of this paper is structured as follows. Section 2 reviews related work, Section 3 details our proposed method, Section 4 presents our empirical evaluation, and Section 5 concludes with key findings and avenues for future research.

2 Related Works

Hyperalignment (HA) is a deterministic alignment technique that uses generalized CCA to enhance prediction accuracy in fMRI analysis [5, 11, 12]. Classic HA's requirement to invert high-dimensional covariance matrices makes it unreliable for highly correlated data—*e.g.*, whole-brain

[2] Available at `https://data-archive.nimh.nih.gov/`

[3] Available at `https://www.humanconnectome.org/`

[4] Available at `https://openneuro.org/`

images; variants such as regularized hyperalignment (RHA) [11], singular value decomposition hyperalignment (SVDHA) [22], and (non-parametric) kernel hyperalignment (KHA) [12] respectively introduce regularization, low-rank decompositions, or kernel mappings to stabilize alignment. Deep hyperalignment (DHA) further extends this line by employing a deep neural network as a learnable kernel to capture complex, nonlinear subject-specific transformations end-to-end [9]. More recently, deep geodesic canonical correlation analysis (DeepGeoCCA) has been proposed to generalize CCA to symmetric positive-definite covariance matrices on Riemannian manifolds, yielding robust covariance-based alignment by maximizing geodesic correlation [13].

SRM offers a probabilistic alternative to HA by aligning neural responses via maximum-likelihood estimation of a shared latent timecourse [10]. Subsequent work introduced a multi-view convolutional autoencoder (CAE + SRM), which leverages convolutional neural networks to extract richer features before alignment [23]. Matrix-Normal SRM (MN-SRM) employs Kronecker-separable covariance priors and maximum a posteriori estimation to jointly model spatial and temporal noise [24], while robust SRM (RSRM) applies sparse, deterministic optimization to disentangle shared and subject-specific components [25]. FastSRM presents an identifiable SRM variant with a dimension-reduction preprocessing step that stabilizes and accelerates shared response recovery, achieving orders-of-magnitude speed-ups without loss of accuracy [6].

Shared independent component analysis (ShICA) replaces the CCA step with independent component analysis (ICA) to learn statistically independent shared components under additive Gaussian noise, improving alignment on data with non-Gaussian artifacts [26]. However, ShICA only models shared variance. To address this, shared and individual ICA (ShIndICA) was proposed to jointly recover both shared and subject-specific sources, with provable identifiability via likelihood-based estimation [3]. Beyond ICA, the hyper hidden Markov model (Hyper-HMM) projects voxels into a latent event space and aligns temporal segments across subjects, enabling joint spatial–temporal correspondence in naturalistic fMRI paradigms [4].

Several multi-site transfer-learning approaches have been developed to harmonize task-based fMRI data across scanners and cohorts, including maximum independence domain adaptation (MIDA) [27], multi-dataset dictionary learning (MDDL) [28], and multi-dataset multi-subject (MDMS) [28], side information dependence regularization (SIDeR) [7]. The shared space transfer learning (SSTL) [1] further extends this line by extracting site-specific common features through a single-iteration multi-view optimization and mapping them into a site-independent shared space, thereby enabling scalable alignment of high-dimensional fMRI data. SSTL can incorporate the deep-kernel formulation introduced in DHA [9]—termed DeepSSTL—to further boost prediction accuracy in multi-site fMRI studies [1]. Explainability-generalizable graph neural networks (XG-GNN) is a meta-learning framework with domain-generalizable explainability regularizers that learns graph neural networks for multi-site fMRI analysis, demonstrating robust cross-center performance and interpretable subgraph discovery [8].

Self-supervised 'constructive' learning methods have recently been applied to multi-view fMRI alignment. Foundational contrastive frameworks such as SimCLR [14], bootstrap-your-own-latent (BYOL) [15], DINO [16], and its successor DINOv2 [17] learn view-invariant representations without labels. In task-based fMRI, MindEye combines contrastive encoding with diffusion priors to reconstruct viewed images while implicitly aligning subjects in the latent space [18]; MindEye2 demonstrates that a shared-subject generative model pretrained across participants can be fine-tuned with just one hour of data to decode images from fMRI [19]. More recently, MindAligner learns explicit cross-subject transformation networks for functional alignment in task-based fMRI [20]. These self-supervised approaches offer promising alternatives for multi-subject alignment by leveraging rich augmentations and momentum-based architectures. In the following, we empirically compare our proposed method to some of these approaches.

3 The Proposed Orthogonal Contrastive Learning (OCL)

This section introduces orthogonal contrastive learning (OCL), a novel multi-view framework for multi-subject fMRI analysis. Similar to previous functional alignment methods, OCL considers each subject's neural responses as a separate view of the same underlying data. As Figure 1 illustrated, OCL employs two neural networks with identical architectures: an online network, which actively learns representations through a contrastive objective, and a target network, whose parameters are gradually updated as a moving average of the online network's parameters. This dual-network

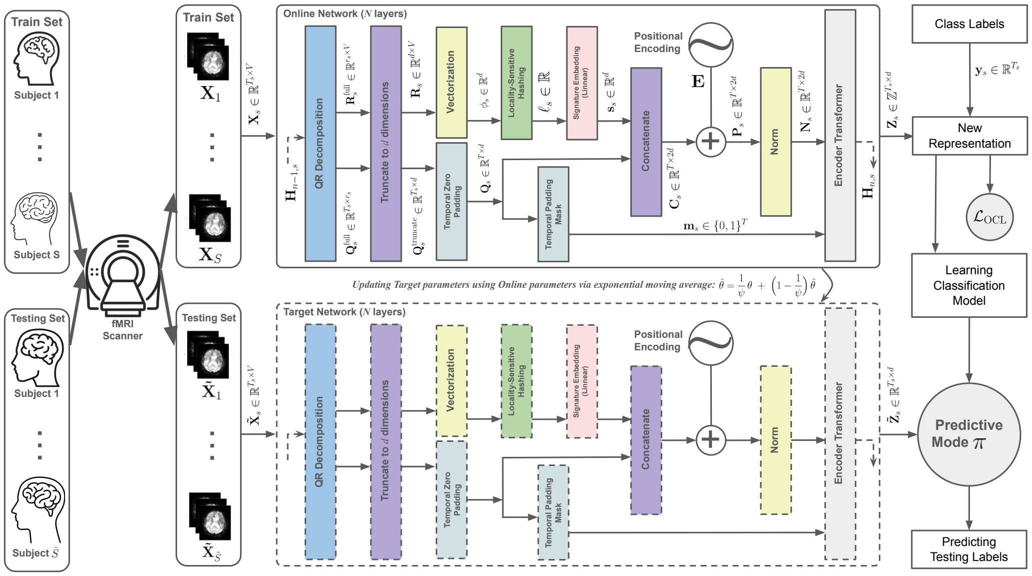
Train Set
Subject 1
Subject S
Testing Set
Subject 1
Subject $\tilde{S}$
fMRI Scanner
Train Set
$\mathbf{X}_1$
$\mathbf{X}_S$
Testing Set
$\tilde{\mathbf{X}}_1$
$\tilde{\mathbf{X}}_{\tilde{S}}$
$\mathbf{X}_s \in \mathbb{R}^{T_s \times V}$
$\tilde{\mathbf{X}}_s \in \mathbb{R}^{T_s \times V}$
Online Network (N layers)
$\mathbf{H}_{n-1,s}$
QR Decomposition
$\mathbf{R}_s^{\text{full}} \in \mathbb{R}^{r_s \times V}$
$\mathbf{Q}_s^{\text{full}} \in \mathbb{R}^{T_s \times r_s}$
Truncate to d dimensions
$\mathbf{R}_s \in \mathbb{R}^{d \times V}$
$\mathbf{Q}_s^{\text{truncate}} \in \mathbb{R}^{T_s \times d}$
Vectorization
$\phi_s \in \mathbb{R}^{\bar{d}}$
Locality-Sensitive Hashing
$\ell_s \in \mathbb{R}$
Signature Embedding (Linnear)
$\mathbf{s}_s \in \mathbb{R}^d$
Temporal Zero Padding
$\mathbf{Q}_s \in \mathbb{R}^{T \times d}$
Temporal Padding Mask
Positional Encoding
$\mathbf{E}$
Concatenate
$\mathbf{C}_s \in \mathbb{R}^{T \times 2d}$
$\mathbf{P}_s \in \mathbb{R}^{T \times 2d}$
Norm
$\mathbf{N}_s \in \mathbb{R}^{T \times 2d}$
$\mathbf{m}_s \in \{0,1\}^T$
Encoder Transformer
$\mathbf{H}_{n,s}$
$\mathbf{Z}_s \in \mathbb{Z}^{T_s \times d}$
Updating Target parameters using Online parameters via exponential moving average: $\tilde{\theta} = \frac{1}{\psi}\theta + \left(1 - \frac{1}{\psi}\right)\tilde{\theta}$
Target Network (N layers)
$\tilde{\mathbf{Z}}_s \in \mathbb{R}^{T_s \times d}$
Class Labels
$\mathbf{y}_s \in \mathbb{R}^{T_s}$
New Representation
$\mathcal{L}_{\text{OCL}}$
Learning Classification Model
Predictive Mode π
Predicting Testing Labels

Figure 1: The Proposed Orthogonal Contrastive Learning (OCL)

setup stabilizes training and ensures consistent representations across subjects. Each OCL layer has four primary components: first, QR decomposition, which yields orthonormal feature bases to decorrelate signals and enhance the signal-to-noise ratio; second, locality-sensitive hashing (LSH), which produces compact subject-specific signatures; third, positional encoding, which integrates fMRI temporal information into spatial feature representations; finally, a transformer encoder integrates these inputs, ensuring that neural representations from the same stimulus become closely aligned, while representations of different stimuli remain distinct. In the remainder of this section, we mathematically define OCL, present a pretraining strategy to improve its performance, and discuss extending OCL through transfer learning for multi-site fMRI analysis.

We let S be the number of subjects in the training set. Let $T_s, s = 1, \dots, S$ denote the number of time points for the s-th subject, and let V be the number of voxels in the selected region of interest (ROI), which we view as a 1D vector, even though it corresponds to a 3D volume. The preprocessed neural responses for the s-th subject is then defined as $\mathbf{X}_s \in \mathbb{R}^{T_s \times V}$. For simplicity, this paper assumes that each column of the neural responses is standardized during preprocessing: $\mathbf{X}_s \sim \mathcal{N}(0, \mathbf{I}),\ s = 1, \dots, S$, $\mathbf{I}$ is the identity matrix. In addition, the v-th column in $\mathbf{X}_s$ for all subjects denotes the anatomically aligned voxel located at the same locus across fMRI images [1]. We then let N defines the number of layers in the online and target networks, $f_n, n = 1, \dots, N$ is the transformations implemented by each layer, and $\mathbf{H}_{n,s} = f_n(\mathbf{H}_{n-1,s}), n = 1, \dots, N, s = 1, \dots, S$ is all transformations applied in the n-th layer of the proposed OCL architecture on the nerual responses of s-th subject. Here, we consider $\mathbf{H}_{0,s} = \mathbf{X}_s$ as input layer of the networks for each subject. Further, we let $r_s = \text{rank}(\mathbf{X}_s)$ denote the rank of the neural response matrix of the s-th subject, and $d \leq \min_{s=1,\dots,S}(r_s)$ be the number of components in the final representation such that $\mathbf{H}_{n,s} \in \mathbb{R}^{T_s \times d}, n = 1, \dots, N, s = 1, \dots, S$, $\mathbf{Z}_s \in \mathbb{R}^{T_s \times d} = \mathbf{H}_{N,s}$ as the final representation of neural representations for each subject that can be used for downstream classification analysis.

The first component in each OCL transformation layer is a QR decomposition. Given the neural response matrix of the s-th subject $\mathbf{X}_s$, we apply thin (reduced) QR decomposition [29] to factor $\mathbf{X}_s = \mathbf{Q}_s^{\text{full}} \mathbf{R}_s^{\text{full}}$, where $\mathbf{Q}_s^{\text{full}} \in \mathbb{R}^{T_s \times r_s}$ is orthonormal and $\mathbf{R}_s^{\text{full}} \in \mathbb{R}^{r_s \times V}$ is upper-triangular. We then truncate these factors by taking the first d columns of $\mathbf{Q}_s^{\text{full}}$ to form $\mathbf{Q}_s^{\text{truncate}} \in \mathbb{R}^{T_s \times d}$ and the first d rows of $\mathbf{R}_s^{\text{full}}$ to form $\mathbf{R}_s \in \mathbb{R}^{d \times V}$. This truncation component ensures that each OCL layer produces exactly d features, where d is usually the maximum number of shared features that can be extracted across all training subjects, as determined by their ranks [30]. We let $T \geq \max_{s=1,\dots,S} T_s$ be the maximum content-window size in the OCL architecture. The temporal zero-padding component adds zero rows to each $\mathbf{Q}_s^{\text{truncate}}$ so that all orthonormal matrices share the common shape $\mathbf{Q}_s \in \mathbb{R}^{T \times d}$. Note that T must be large enough to accommodate the neural responses of every subject, including those in the testing set. We also define a binary mask vector $\mathbf{m}_s \in \{0, 1\}^T$, where a value of 1 indicates an actual response time point and 0 indicates padding. We also let $\bar{d}$ be the number of nonzero elements of the upper-triangular matrix $\mathbf{R}_s$ and define $\phi_s \in \mathbb{R}^{\bar{d}} = \mathrm{vec}(\mathbf{R}_s)$ as the vectorization operator that extracts the nonzero elements of the upper-triangular matrix into a single vector, which is then used in the next step to produce subject-specific signatures.

Locality-sensitive hashing (LSH) component is a randomized, data-independent hashing scheme for approximate nearest neighbor search in high-dimensional spaces, ensuring that similar items collide with higher probability than dissimilar ones [21]. We let the parameter $p \in (0, 2]$ be the stability exponent [21, 31], $\mathbf{a} \in \mathbb{R}^{\bar{d}}$ is drawn from a p-stable (Gaussian) distribution, $w \in \mathbb{R}_{>0}$ be the quantization granularity of the hash bins, and $b \sim \mathrm{U}[0, w]$, yielding provable locality sensitivity [21, 32]. We denote the LSH for s-th subject as follows:

$$\ell_s \; = \; \mathrm{lsh}_{\{\mathbf{a},b,w\}}(\phi_s) \; = \; \left\lfloor \frac{\langle \mathbf{a},\, \phi_s \rangle \; + \; b}{w} \right\rfloor, \tag{1}$$

where $\lfloor\rfloor$ is the floor function. Note that LSH is identical for all neural responses of the s-th subject and needs only be computed once for all time points belonging to that subject in each training iteration. We then use a linear multilayer perceptron (MLP) that accepts the scalar $\ell_s \in \mathbb{R}$ as input and produces the vector $\mathbf{s}_s \in \mathbb{R}^d$ as the subject-specific signature (embedding) for the s-th subject.

Lemma 1. *Let each neural responses matrix admit a reduced QR factorization* $\mathbf{X}_s = \mathbf{Q}_s\, \mathbf{R}_s$ *with* $\mathbf{Q}_s^\top \mathbf{Q}_s = \mathbf{I}$. *Define* $\boldsymbol{\phi}_s = \mathrm{vec}(\mathbf{R}_s) = \mathrm{vec}\big(\mathbf{Q}_s^\top\, \mathbf{X}_s\big)$. *If*

$$\big\|\boldsymbol{\phi}_1 - \boldsymbol{\phi}_2\big\| < \big\|\boldsymbol{\phi}_1 - \boldsymbol{\phi}_3\big\| \to \Pr\big[\ell_1 = \ell_2\big] \; > \; \Pr\big[\ell_1 = \ell_3\big].$$

Please refer to the supplementary material for the proof.

We let $\mathbf{C}_s \in \mathbb{R}^{T \times 2d}$ be the output of the concatenation component, which combines each row of the orthonormal matrix $\mathbf{Q}_s \in \mathbb{R}^{T \times d}$ with the subject-specific signature $\mathbf{s}_s \in \mathbb{R}^d$. We then apply a sinusoidal positional encoding to embed temporal context alongside the spatial and signature features. Concretely, we construct a positional encoding matrix

$$\mathbf{E} \in \mathbb{R}^{T \times 2d} = [e_{1,0}, \ldots, e_{T,2d}], \quad e_{t,2i} = \sin\!\Big(\frac{t}{T^{2i/(2d)}}\Big), \quad e_{t,2i+1} = \cos\!\Big(\frac{t}{T^{2i/(2d)}}\Big),$$

for $t = 1, \ldots, T$ and $i = 0, \ldots, d-1$. Adding this to the concatenated features yields the component $\mathbf{P}_s \;\in\; \mathbb{R}^{T \times 2d} = \mathbf{C}_s + \mathbf{E}$, which now encodes both spatial patterns and their temporal positions. Next, OCL applies a normalization component to stabilize and scale each time-step embedding, *i.e.*, given the positional-encoded features $\mathbf{P}_s \in \mathbb{R}^{T \times 2d}$, we compute the normalization $\mathbf{N}_s \in \mathbb{R}^{T \times 2d} = \mathrm{Norm}\big(\mathbf{P}_s\big)$. Finally, these normalized embeddings are passed, together with the temporal padding mask $\mathbf{m}_s$, into a standard Transformer encoder [33] to produce corresponding layer output $\mathbf{H}_{n,s}$.

We let $\mathbf{y}_s = [y_{s,1}, \ldots, y_{s,T_s}]^\top \in \mathbb{R}^{T_s}$ denote the class labels for the s-th subject in the training set. For the s-th subject, let $\mathbf{Z}_s = [z_{s,1}, \ldots, z_{s,T_s}]^\top \in \mathbb{R}^{T_s \times d}$ be the output of final layer of the OCL online network. We define the contrastive loss $\mathcal{L}_{\mathrm{OCL}}(\mathbf{Z}_s, \mathbf{y}_s)$ with temperature τ, margin μ, and between-class weight λ for s-th subject as

$$\begin{aligned}\mathcal{L}_{\mathrm{OCL}\{\tau,\,\mu,\,\lambda\}}(\mathbf{Z}_s, \mathbf{y}_s) = -\frac{1}{T_s}\sum_{i=1}^{T_s} \log \frac{\displaystyle\sum_{\substack{j=1\\ j\neq i,\, y_{s,j}=y_{s,i}}}^{T_s} \exp\big(\langle z_{s,i},\, z_{s,j}\rangle/\tau\big)}{\displaystyle\sum_{k=1}^{T_s} \exp\big(\langle z_{s,i},\, z_{s,k}\rangle/\tau\big)} \\ +\lambda\, \frac{1}{T_s^2}\sum_{i=1}^{T_s}\; \sum_{\substack{j=1\\ y_{s,j}\neq y_{s,i}}}^{T_s} \log\Big(1 + \exp\big(\langle z_{s,i},\, z_{s,j}\rangle/\tau \;-\; \mu\big)\Big).\end{aligned} \tag{2}$$

Let θ denotes all learnable parameters of the online encoder and $\tilde{\theta}$ those of the target encoder. In each training iteration for subject s, we first update the online parameters by one step of gradient descent on the subject's contrastive loss: $\theta \;\leftarrow\; \theta \;-\; \eta\, \nabla_\theta \mathcal{L}_{\mathrm{OCL}}(\mathbf{Z}_s, \mathbf{y}_s)$, η is the learning rate. We update the online network using all subjects in the training set during each iteration. Once the online network has processed every subject's data in each iteration, we update the target network parameters using an exponential moving average (EMA) of the online parameters as follows [15]:

$$\tilde{\theta} = \frac{1}{\psi}\,\theta \;+\; \Big(1 - \frac{1}{\psi}\Big)\,\tilde{\theta}, \tag{3}$$

Table 1: The fMRI datasets

ID	Title	Type	S	$\|\mathbf{y}\|$	T_s	*Site(#)*
A*	Stop signal (DS007) [34]	Decision	20	4	472	B (3)
B	Conditional stop signal (DS008) [35]	Decision	13	4	317	A (1)
CMU	Meanings of Nouns [36]	Semantic	9	12	402	
C	Simon task (DS101) (unpublished [7])	Simon	21	2	302	D (1)
D	Flanker task (DS102) [37]	Flanker	26	2	292	C (1)
DS232	Face-coding models with individual-face [38]	Visual	10	4	760	
E	Integration of sweet taste: Study 1 (DS229) [39]	Flavour	15	6	580	F (1)
F	Integration of sweet taste: Study 3 (DS231) [39]	Flavour	9	6	650	E (1)
Forrest	Forrest Gump movie [40]	Visual	20	10	451	
Raiders	Raiders movie [5, 10]	Visual	10	7	924	

S is the number of subjects; $|\mathbf{y}|$ is the number of stimulus categories; T_s is the number of time points per subject; *Site* lists the other datasets whose neural responses can be transferred to this dataset. # represents the number of sites in the corresponding dataset. * this dataset is partitioned into three independent 'sites'—pseudo-word naming (A1), letter naming (A2), and manual response (A3) [1]

where ψ is the number of total iterations. In the training phase, OCL learns a shared representation space in which neural recordings from all training subjects are aligned. We then train a classifier (denoted by π in Figure 1) on these new representations. In the testing phase, we use the trained target network to map the test data into the same representation space and then apply the classifier to predict cognitive states. We provide the pseudocode for the proposed OCL algorithm in the supplementary material.

3.1 General Pretrained Orthogonal Contrastive Model

To bootstrap OCL for real task-based fMRI, we first pretrain the dual-encoder entirely on synthetic data that mimics the statistical structure of neural timecourses. Concretely, given k class categories, we generate a corpus of random base matrices $\mathbf{M} \in \mathbb{R}^{T\times V}$, where each group of $\frac{T}{k}$ rows is drawn *i.i.d.* from one of k distinct Gaussian distributions with randomly initialized means and variances that differ across distributions. For each base matrix $\mathbf{M}$, we then create S distinct 'views' by applying S random orthonormal rotations: $\mathbf{X}_s = \mathbf{M}\,\mathbf{U}_s, \quad \mathbf{U}_s^\top \mathbf{U}_s = I, \quad s = 1, \dots, S$. Since each row of $\mathbf{M}$ is sampled from one of the k distributions, we assign a corresponding class label $y = k$ to that row, and this label is preserved across all rotated views $\{\mathbf{X}_s\}_{s=1}^{S}$. Each view $\mathbf{X}_s$ is passed through the OCL layers to produce embeddings $\mathbf{Z}_s$, *i.e.*, the contrastive objective pulls together embeddings of the same label across different rotations and pushes apart embeddings of different labels. After pretraining, we transfer the *target* encoder's parameters $\tilde{\theta}$ to initialize the downstream OCL model on the real fMRI data. This EMA-smoothed encoder has already learned to factor out arbitrary orthogonal transforms and subject-specific variability, providing a strong, generalizable starting point for aligning real neural data with minimal additional tuning.

Lemma 2. *Let each synthetic view be generated by an orthonormal rotation of the base data,* $\mathbf{X}_s = \mathbf{M}\,\mathbf{U}_s, \quad \mathbf{U}_s^\top \mathbf{U}_s = \mathbf{I}$. *Write the corresponding QR factor* $\mathbf{R}_s$ *and its flattened vector* $\boldsymbol{\phi}_s = \mathrm{vec}(R_s)$. *Then for any three views* $\mathbf{X}_1, \mathbf{X}_2, \mathbf{X}_3$ *generated from* $\mathbf{M}$*,*

$$\Pr\big[\ell_1 = \ell_2\big] \;=\; \Pr\big[\ell_1 = \ell_3\big].$$

In other words, the collision probability of the LSH hash is identical across all random rotations generated from $\mathbf{M}$.

Please see the supplementary material for the proof.

3.2 Transfer Learning via Orthogonal Contrastive Embeddings

To extend OCL to multi-site fMRI studies, suppose we have B training sites, each providing data $\{\mathbf{X}_s^{(b)}, \mathbf{y}_s^{(b)}\}_{s=1}^{S_b}$ for site $b = 1, \dots, B$. We train an independent OCL instance on each site, yielding target-encoder parameters $\tilde{\theta}_b,\ b = 1, \dots, B$. These *site-specific* encoders capture local scanner and population idiosyncrasies while maintaining the shared contrastive objective. To initialize OCL on a multi-site setup (with no extra fine-tuning step), we aggregate the B learned targets via

$$\tilde{\theta}_{\text{sites}} \;=\; \frac{1}{B}\sum_{b=1}^{B} \tilde{\theta}_b, \tag{4}$$

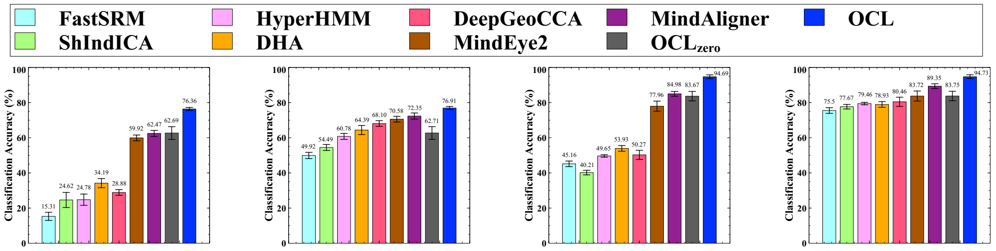

(a) CMU (Temporally Unaligned) (b) CMU (Temporally Aligned) (c) DS232 (Temporally Unaligned) (d) DS232 (Temporally Aligned)

Figure 2: Classification analysis on Temporally Aligned versus Temporally Unaligned Data. Plotted are mean accuracies and error bars are ±1 standard deviation.

thereby blending all site-specific knowledge into a single robust prior. We then freeze $\tilde{\theta}_{\text{sites}}$ and apply it to both the training-site and testing-site data, projecting each into the same shared feature space defined by the aggregated targets—this alignment boosts the accuracy of our downstream classifiers.

Please note that this multi-site adaptation scheme also enables an active learning loop in the real world applications. At each iteration, we evaluate the contrastive loss $\mathcal{L}_{\text{OCL}}^{(\bar{b})}$ on the predicted time points from the testing site $\bar{b}$ and select those with highest uncertainty (*e.g.*, largest margin-based loss) for expert manual labeling. The newly annotated samples are then incorporated into the training set, the online encoder parameters are updated accordingly, and the target encoder is refined via EMA. By focusing annotation effort on the most informative temporal segments, this closed-loop procedure maximizes performance gains in low-data or high-cost labeling scenarios. Although active learning offers a promising avenue for extending OCL, it is beyond the scope of this study; all reported results were obtained without active-learning or expert-annotated data.

4 Experiments

Table 1 summarizes the 10 datasets used in our empirical evaluation. Datasets CMU and DS232 consist of simple cognitive task-prediction paradigms, whereas Forrest and Raiders datasets involve naturalistic movie-watching stimuli in single-site fMRI studies. We also include 6 homogeneous task-based fMRI datasets (A–F) suitable for multi-site analysis. All datasets are publicly available (via OpenNEURO [4], except CMU [5]) and were preprocessed with our GUI-based toolbox called easy fMRI [6] and FSL 6.0.15 [7], including spatial normalization, smoothing, anatomical alignment; for those alignment techniques that require it, temporal realignment was also applied (see Section 4.1). Each scan was registered to the MNI152 T1-weighted template [1] at a $4mm$ isotropic resolution, and a whole-brain ROI was defined for all analyses, yielding $V = 19{,}742$ voxels per volume. Data were standardized during preprocessing, without loss of generality.

We benchmark OCL against 7 single-site fMRI analysis methods: FastSRM and HyperHMM as baselines; ShIndICA as a non-CCA method; DHA and DeepGeoCCA as deep multi-view learning approaches; and MindEye2 and MindAligner as self-supervised constructive learning approaches. For multi-site evaluation, we compare OCL to 5 existing techniques: SSTL as a baseline; DeepSSTL and XG-GNN as deep multi-site learning approaches; and MindEye2 and MindAligner as self-supervised constructive methods. Crucially, each site's data are strictly partitioned so that no neural responses from a given site appear in both the training and testing sets. All experiments were run on two PCs with the specifications listed in the Footnote [8]. Our proposed OCL algorithm is available on GitHub [9]. Like the previous studies [1, 9, 10], we employ a ν-support vector machine (ν-SVM) [41] for all classification experiments. We use a leave-one-subject-out nested cross-validation: in each outer fold, one subject is held out for testing; within each, another subject serves as validation (inner fold), and the rest form the training set. Hyperparameters for alignment and ν-SVM (*e.g.*, RBF kernel scale, ν) are selected via grid search on validation accuracy, and the best testing accuracy is reported for each technique.

[5] Available at `https://www.cs.cmu.edu/afs/cs.cmu.edu/project/theo-81/www/`

[6] Available at `https://easyfmri.learningbymachine.com/`

[7] Available at `https://fsl.fmrib.ox.ac.uk/fsl`

[8] OS: Fedora 42, Python: 3.11.9, PyTorch: 2.6, CUDA: 12.6; Connection: 2×40GbE CX314A Mellanox
(PC1) CPU: AMD EPYC 7551P (64 cores), RAM: 256G GPU:2×NVIDIA 4060Ti 16G;
(PC2) CPU: AMD Threadripper 2990WX (64 cores), RAM: 128G, GPU:2×NVIDIA 4060Ti 16G.

[9] OCL code repository: `https://github.com/myousefnezhad/ocl`

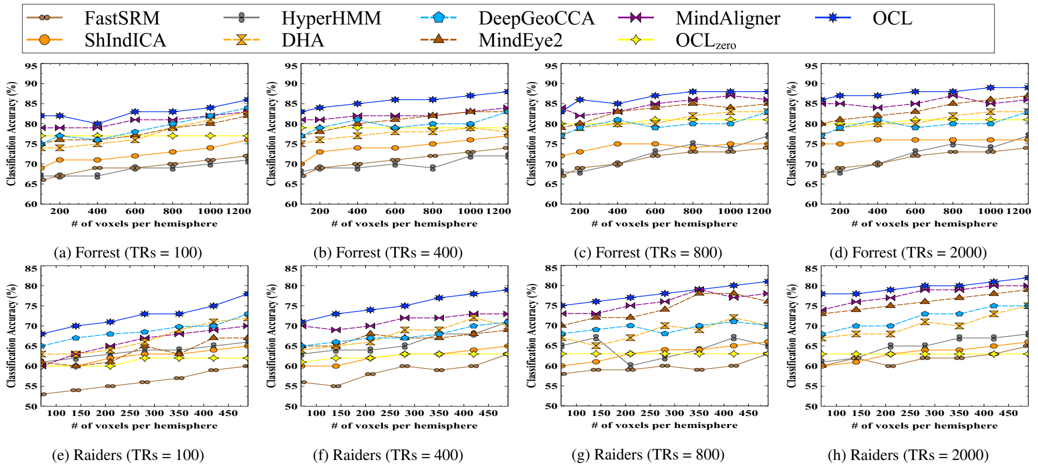

(a) Forrest (TRs = 100)

(b) Forrest (TRs = 400)

(c) Forrest (TRs = 800)

(d) Forrest (TRs = 2000)

(e) Raiders (TRs = 100)

(f) Raiders (TRs = 400)

(g) Raiders (TRs = 800)

(h) Raiders (TRs = 2000)

Figure 3: Classification analysis on movie stimuli. Potted are mean accuracies.

For OCL, we first initialize a model (‘OCL$_{\text{zero}}$’) by pretraining on two million ($4 \times 500{,}000$) synthetic matrices $\mathbf{M} \in \mathbb{R}^{T \times V}$ for $k \in \{5, 10, 20, 50\}$ categories with $T = 2000$ time points and $V = 19742$ voxels, each subjected to $S = 360$ random rotations. We set the embedding dimension to $d = 256$, employ Encoding Transformer with 16 attention heads, and use $N = 32$ network layers. These hyperparameters were chosen to balance representational capacity with available computational resources listed in the Footnote [8]. We then initialize each OCL instance with the pretrained target encoder $\tilde{\theta}$, and fine-tune both online and target networks on the real fMRI data. We train (and pretrain) OCL for up to $\psi = 1000$ iterations with automatic early stopping based on validation loss using Adam optimizer [42]. At each iteration, we form a batch from all time points of a single subject—treating each time point as an independent sample—and randomly shuffle their order. This permutation prevents the network from overfitting to a fixed temporal sequence and encourages robustness to varied response orderings. Because every fine-tuned OCL model is initialized from OCL$_{\text{zero}}$, we employ the same OCL network architecture across all experiments in this paper. OCL consistently produces a feature space of dimension $d = 256$. For all competing methods, we evaluate two latent space sizes—one fixed at $d = 256$ and a second chosen via grid search—and report the configuration that yields the highest classification accuracy. Other self-supervised approaches are similarly initialized with their published pretrained weights [19, 20]. All remaining hyperparameters for both the alignment and classification models are optimized using grid search. We perform grid search over the key OCL hyperparameters — temperature $\tau \in \{0.01, 0.1, 0.5, 0.9, 0.99\}$, margin $\mu \in \{0.1, 0.2, 0.5, 0.8, 0.9\}$, between-class weight $\lambda \in \{0.1, 0.2, 0.3, 0.4, 0.5\}$, learning rate $\eta \in \{0.1, 0.2, 0.3, 0.4\}$, and quantization granularity $w \in \{0.9, 1.0, 1.1, 1.2\}$ — and select the combination that maximizes performance on the validation set.

4.1 Simple Cognitive Task Classification: Temporally Aligned *vs.* Unaligned Data

This section evaluates OCL on two simple cognitive-task datasets (CMU and DS232), in which subjects performed Semantic, and Visual assessments during fMRI scanning. Unlike most functional alignment methods—which assume temporal synchronization (*i.e.*, each time point t corresponds to the same stimulus across subjects)—OCL can handle varying time-series lengths and arbitrary time-point ordering without explicit temporal preprocessing. We therefore compare OCL and several alignment techniques both on the raw, unaligned data and after applying their required temporal alignment. To robustly tune and assess performance, we employ a nested leave-one-subject-out procedure: in each outer fold one subject is held out for testing, while in each inner fold a different subject is held out for validation and hyperparameter selection. Figure 2 shows that traditional alignment methods suffer significant testing accuracy degradation on unaligned data because their shared-space templates misalign stimuli across rows; in contrast, self-supervised constructive approaches (MindEye2, MindAligner, and OCL) learn flexible mappings rather than fixed templates, yielding stable shared representations. OCL in particular achieves the highest accuracy, likely due to (1) its orthogonal decomposition of independent versus subject-specific features and (2) the pretrained ‘OCL$_{\text{zero}}$’ encoder’s ability to generalize arbitrary rotations to novel neural patterns. Each of the 4 plots in Figure 2 is comparing OCL with 7 different methods $\chi = \{$FastSRM, ShIndICA,

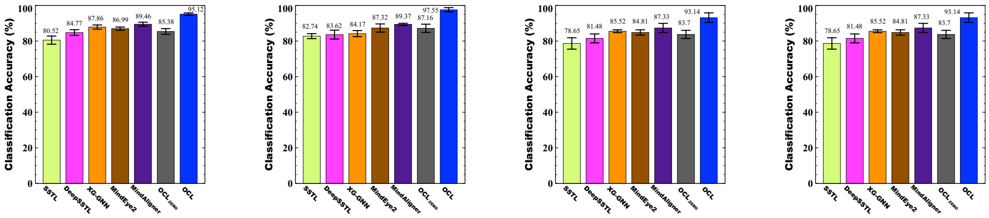

(a) A ⇌ B (b) C ⇌ D (c) E ⇌ F (d) Pairs of {A1, A2, A3, B}

Figure 4: Multi-site Classification Analysis. Plotted are mean accuracies and error bars are ±1 standard deviation.

HyperHMM, DHA, DeepGeoCCA, MindEye2, MindAligner} for a total of $4 \times 7 = 28$ comparisons — where the 2-sided t-test found $\rho < 0.05$ in all 28 cases.

4.2 Classification Analysis on Movie Stimuli

This section evaluates functional alignment techniques on the two movie-watching fMRI datasets (Forrest and Raiders) listed in Table 1, using the same nested leave-one-subject-out scheme as in Section 4.1. Following the procedure of [5], we first rank voxels within the predefined ROI by their task-evoked activation strength, as in [9, 10, 30]. We then assess each alignment method across multiple spatial resolutions by selecting the top $\{100, 200, 400, 600, 800, 1000, 1200\}$ voxels for Forrest and $\{70, 140, 210, 280, 350, 420, 490\}$ voxels for Raiders. To test temporal coverage, we further repeat all experiments using the first $\{100, 400, 800, 2000\}$ Time of Repetitions (TRs) of each scan. Note that in OCL, voxels outside the ROI are zeroed out in the input layer, and the subsequent QR decomposition automatically ignores these zeros, preventing them from influencing the learned representations. Figure 3 presents classification accuracy as a function of voxel count and number of time points, comparing our proposed OCL to 7 alignment approaches $\chi = \{\text{FastSRM}, \text{ShIndICA}, \text{HyperHMM}, \text{DHA}, \text{DeepGeoCCA}, \text{MindEye2}, \text{MindAligner}\}$ for a total of $8 \times 7 \times 7 = 392$ pairwise evaluations. Self-supervised methods initialized with pretrained models typically outperform traditional functional-alignment techniques. In every evaluation, OCL surpasses all comparators—an advantage we attribute to its orthogonal feature decomposition and contrastive alignment. A two-sided t-test confirms that the accuracy differences are significant ($\rho < 0.05$) in all 392 comparisons.

4.3 Multi-Site Classification Analysis

This section presents the results of multi-site fMRI analyses using datasets A–F listed in Table 1. For each pair of sites (A, B), we conducted a two-sided cross-site evaluation: in the forward direction $A \rightarrow B$, we trained and validated alignment and classification models using site A and evaluated them on site B; in the reverse direction $B \rightarrow A$, we reversed the training and testing roles. The final accuracy is computed as the mean of both directions. This bidirectional setup is denoted as $A \rightleftharpoons B$. Figures 4 (a–c) summarize the classification accuracies across multiple cross-site pairs. In addition, Figure 4 (d) presents the mean accuracy of supplementary experiments based on all possible two-versus-two train/test splits derived from the set {A1, A2, A3, B}, yielding six distinct comparisons[10]—for example, training on {A1, A2} and testing on {A3, B}, and vice versa. As shown, the baseline method SSTL, which relies on linear transformations, consistently underperforms. In contrast, DeepSSTL improves accuracy by utilizing a MLP based deep kernel for alignment. Constructive learning approaches further enhance accuracy by leveraging pretrained models that better generalize across domains. The proposed OCL framework achieves the highest classification performance across all site-pairs. This improvement appears to stem from two key design elements: (1) the use of a pretrained multi-representational alignment module that provides a robust initial feature space, and (2) a specialized architecture that enforces cross-site shared information via a contrastive loss. Each of the 4 subplots in Figure 4 compares OCL against a competing method χ, for each of five baselines $\chi \in \{\text{SSTL}, \text{DeepSSTL}, \text{XG-GNN}, \text{MindEye2}, \text{MindAligner}\}$, resulting in a total of $4 \times 5 = 20$ comparisons. In all cases, a two-sided paired t-test yielded statistically significant differences ($\rho < 0.05$), confirming the robustness of OCL in cross-site generalization.

[10] Pairs: {A1, A2}, {A1, A3}, {A1, B}, {A2, A3}, {A2, B}, {A3, B}

5 Conclusion

This paper has introduced orthogonal contrastive learning (OCL), a unified framework that addresses task-based fMRI's key challenges: low signal-to-noise ratio, high dimensionality, and variable time-series lengths. OCL aligns neural responses across subjects and sites without explicit temporal preprocessing. OCL employs a dual-encoder design: an online network and a target network whose weights track the online network via exponential moving average to stabilize learning. Each OCL network layer combines QR decomposition for orthogonal feature extraction, locality-sensitive hashing (LSH) to produce compact subject-specific signatures, positional encoding to embed temporal structure alongside spatial features, and a transformer encoder to generate discriminative, stimulus-aligned embeddings, trained with a contrastive loss that pulls together same-stimulus responses and pushes apart different-stimulus responses. We further enhance OCL with an unsupervised pretraining stage on fMRI-like synthetic data and demonstrate a transfer-learning workflow for multi-site studies. Across extensive experiments on multi-subject and multi-site fMRI benchmarks, OCL consistently outperforms state-of-the-art alignment and analysis methods in both representation quality and downstream classification accuracy.

In the future, OCL has the potential to be applied across a variety of task-based fMRI studies, such as reconstructing visual stimuli or movies from human brain activity, as well as extended to other neuroimaging modalities including resting-state fMRI, MEG, and EEG. For resting-state fMRI, pseudo-labels can be generated by applying sliding-window functional connectivity or by clustering temporal windows based on correlation patterns; OCL can then maximize contrastive agreement across these pseudo-classes, effectively aligning subjects in the absence of explicit tasks. Similarly, for MEG and EEG data, the decomposition can operate on sensor- or source-space time series, while LSH can hash spectral or time–frequency representations. Positional encoding further preserves temporal ordering, even when sampling rates vary across modalities. Moreover, OCL can be scaled to larger voxel spaces and multi-site datasets, paving the way toward a foundation model for fMRI analysis—although such scaling would require substantial GPU cluster resources.

6 Broader Impacts

Orthogonal contrastive learning (OCL) enables large-scale pooling of multi-site fMRI datasets, substantially improving statistical power and reproducibility by harmonizing site-specific biases and reducing variance in group-level inferences. By aligning subject-specific neural signatures into a shared space, OCL facilitates the discovery of robust biomarkers for neurological and psychiatric disorders, advancing precision psychiatry and personalized medicine. Eliminating the need for explicit temporal preprocessing and uniform time-series lengths, OCL lowers technical barriers to integrating diverse datasets, supporting open-science platforms and accelerating collaborative research. Finally, by democratizing access to high-quality, reproducible fMRI representations and mitigating batch effects, OCL promotes ethical, transparent AI-driven neuroscience, fostering cross-disciplinary innovation and responsible research practices.

7 Limitations

OCL's multi-module architecture enables strong alignment but comes with important caveats: (i) Computation: its dual-network and Transformer components demand substantially greater computation power than traditional alignment methods, limiting scalability to very high-dimensional feature spaces; (ii) Domain shift: performance may degrade under extreme inter-site or inter-subject domain shifts beyond those in our benchmarks; (iii) Data requirements: its ability to generalize robustly hinges on access to large, well-annotated multi-site datasets, constraining usefulness in small-sample or weakly labeled settings; and (iv) Interpretability: deep learning in neuroimaging is not easily interpretable, and while we provide initial insights via QR-basis spatial projections and attention maps, comprehensive interpretability is outside the scope of this work.

Acknowledgments

I would like to express my sincere gratitude to Stephen P. Kaiser of the National Bank of Canada for his generous support in the publication of this research study.

References

[1] Tony Muhammad Yousefnezhad, Alessandro Selvitella, Daoqiang Zhang, Andrew Greenshaw, and Russell Greiner. Shared space transfer learning for analyzing multi-site fmri data. *Advances in Neural Information Processing Systems (NeurIPS)*, 33:15990–16000, 2020.

[2] Shuo Huang, Liang Sun, Muhammad Yousefnezhad, Meiling Wang, and Daoqiang Zhang. Functional alignment-auxiliary generative adversarial network-based visual stimuli reconstruction via multi-subject fmri. *IEEE Transactions on Neural Systems and Rehabilitation Engineering*, 31:2715–2725, 2023.

[3] Teodora Pandeva and Patrick Forré. Multi-view independent component analysis with shared and individual sources. In *Uncertainty in Artificial Intelligence*, pages 1639–1650. PMLR, 2023.

[4] Caroline Lee, Jane Han, Ma Feilong, Guo Jiahui, James Haxby, and Christopher Baldassano. Hyper-hmm: aligning human brains and semantic features in a common latent event space. *Advances in Neural Information Processing Systems (NeurIPS)*, 36:27005–27019, 2023.

[5] James V Haxby, J Swaroop Guntupalli, Andrew C Connolly, Yaroslav O Halchenko, Bryan R Conroy, M Ida Gobbini, Michael Hanke, and Peter J Ramadge. A common, high-dimensional model of the representational space in human ventral temporal cortex. *Neuron*, 72(2):404–416, 2011.

[6] Hugo Richard and Bertrand Thirion. Fastsrm: A fast, memory efficient and identifiable implementation of the shared response model. *Aperture Neuro*, 2023.

[7] Shuo Zhou, Wenwen Li, Christopher Cox, and Haiping Lu. Side information dependence as a regularizer for analyzing human brain conditions across cognitive experiments. In *Proceedings of the AAAI Conference on Artificial Intelligence (AAAI)*, volume 34:04, pages 6957–6964, 2020.

[8] Xinmei Qiu, Fan Wang, Yongheng Sun, Chunfeng Lian, and Jianhua Ma. Towards graph neural networks with domain-generalizable explainability for fmri-based brain disorder diagnosis. In *International Conference on Medical Image Computing and Computer-Assisted Intervention (MICCAI)*, pages 454–464. Springer, 2024.

[9] Muhammad Yousefnezhad and Daoqiang Zhang. Deep hyperalignment. In *Advances in Neural Information Processing Systems (NIPS)*, pages 1603–1611, 2017.

[10] Po Hsuan Cameron Chen, Janice Chen, Yaara Yeshurun, Uri Hasson, James Haxby, and Peter J Ramadge. A reduced-dimension fmri shared response model. In *Advances in Neural Information Processing Systems (NIPS)*, pages 460–468, 2015.

[11] Hao Xu, Alexander Lorbert, Peter J Ramadge, J Swaroop Guntupalli, and James V Haxby. Regularized hyperalignment of multi-set fmri data. In *IEEE Statistical Signal Processing Workshop (SSP)*, pages 229–232. IEEE, 2012.

[12] Alexander Lorbert and Peter J Ramadge. Kernel hyperalignment. In *Advances in Neural Information Processing Systems (NIPS)*, pages 1790–1798, 2012.

[13] Ce Ju, Reinmar J Kobler, Liyao Tang, Cuntai Guan, and Motoaki Kawanabe. Deep geodesic canonical correlation analysis for covariance-based neuroimaging data. In *International Conference on Learning Representations (ICLR)*, 2024.

[14] Ting Chen, Simon Kornblith, Mohammad Norouzi, and Geoffrey Hinton. A simple framework for contrastive learning of visual representations. In *International Conference on Machine Learning (ICML)*, pages 1597–1607. PMLR, 2020.

[15] Jean-Bastien Grill, Florian Strub, Florent Altché, Corentin Tallec, Pierre Richemond, Elena Buchatskaya, Carl Doersch, Bernardo Avila Pires, Zhaohan Guo, Mohammad Gheshlaghi Azar, et al. Bootstrap your own latent-a new approach to self-supervised learning. *Advances in Neural Information Processing Systems (NeurIPS)*, 33:21271–21284, 2020.

[16] Mathilde Caron, Hugo Touvron, Ishan Misra, Hervé Jégou, Julien Mairal, Piotr Bojanowski, and Armand Joulin. Emerging properties in self-supervised vision transformers. In *Proceedings of the IEEE/CVF International Conference on Computer Vision*, pages 9650–9660, 2021.

[17] Maxime Oquab, Timothée Darcet, Théo Moutakanni, Huy Vo, Marc Szafraniec, Vasil Khalidov, Pierre Fernandez, Daniel Haziza, Francisco Massa, Alaaeldin El-Nouby, et al. Dinov2: Learning robust visual features without supervision. *Transactions on Machine Learning Research Journal*, 2024.

[18] Paul Scotti, Atmadeep Banerjee, Jimmie Goode, Stepan Shabalin, Alex Nguyen, Aidan Dempster, Nathalie Verlinde, Elad Yundler, David Weisberg, Kenneth Norman, et al. Reconstructing the mind's eye: fmri-to-image with contrastive learning and diffusion priors. *Advances in Neural Information Processing Systems (NeurIPS)*, 36:24705–24728, 2023.

[19] Paul S Scotti, Mihir Tripathy, Cesare Kadir Torrico Villanueva, Reese Kneeland, Tong Chen, Ashutosh Narang, Charan Santhirasegaran, Jonathan Xu, Thomas Naselaris, Kenneth A Norman, et al. Mindeye2: shared-subject models enable fmri-to-image with 1 hour of data. In *Proceedings of the International Conference on Machine Learning (ICML)*, pages 44038–44059, 2024.

[20] Yuqin Dai, Zhouheng Yao, Chunfeng Song, Qihao Zheng, Weijian Mai, Kunyu Peng, Shuai Lu, Wanli Ouyang, Jian Yang, and Jiamin Wu. Mindaligner: Explicit brain functional alignment for cross-subject visual decoding from limited fmri data. *arXiv preprint arXiv:2502.05034*, 2025.

[21] Mayur Datar, Nicole Immorlica, Piotr Indyk, and Vahab S Mirrokni. Locality-sensitive hashing scheme based on p-stable distributions. In *Proceedings of Symposium on Computational Geometry (SoCG)*, pages 253–262, 2004.

[22] Po Hsuan Chen, J Swaroop Guntupalli, James V Haxby, and Peter J Ramadge. Joint svd-hyperalignment for multi-subject fmri data alignment. In *IEEE International Workshop on Machine Learning for Signal Processing (MLSP)*, pages 1–6. IEEE, 2014.

[23] Po-Hsuan Chen, Xia Zhu, Hejia Zhang, Javier S Turek, Janice Chen, Theodore L Willke, Uri Hasson, and Peter J Ramadge. A convolutional autoencoder for multi-subject fmri data aggregation. *29th Workshop of Representation Learning in Artificial and Biological Neural Networks*, 2016.

[24] Michael Shvartsman, Narayanan Sundaram, Mikio Aoi, Adam Charles, Theodore Willke, and Jonathan Cohen. Matrix-normal models for fmri analysis. In *International Conference on Artificial Intelligence and Statistics (AISTAT)*, pages 1914–1923. PMLR, 2018.

[25] Javier S Turek, Cameron T Ellis, Lena J Skalaban, Nicholas B Turk-Browne, and Theodore L Willke. Capturing shared and individual information in fmri data. In *IEEE International Conference on Acoustics, Speech and Signal Processing (ICASSP)*, pages 826–830. IEEE, 2018.

[26] Hugo Richard, Pierre Ablin, Bertrand Thirion, Alexandre Gramfort, and Aapo Hyvarinen. Shared independent component analysis for multi-subject neuroimaging. *Advances in Neural Information Processing Systems (NeurIPS)*, 34:29962–29971, 2021.

[27] Ke Yan, Lu Kou, and David Zhang. Learning domain-invariant subspace using domain features and independence maximization. *IEEE Transactions on Cybernetics*, 48(1):288–299, 2017.

[28] Hejia Zhang, Po-Hsuan Chen, and Peter Ramadge. Transfer learning on fmri datasets. In *International Conference on Artificial Intelligence and Statistics (AISTATS)*, pages 595–603. PMLR, 2018.

[29] Gene H Golub and Charles F Van Loan. Matrix computations, 2013.

[30] Muhammad Yousefnezhad, Alessandro Selvitella, Liangxiu Han, and Daoqiang Zhang. Supervised hyperalignment for multi-subject fmri data alignment. *IEEE Transactions on Cognitive and Developmental Systems (TCDS)*, 2020.

[31] Hongkai Nguyen. Lecture notes: Sketching and p-stable distributions. CS261, Stanford University, 2019. Definition 2.1.

[32] Pinecone Systems, Inc. Pinecone: Vector database for scalable similarity search. `https://www.pinecone.io`, 2025. Accessed: 2025-05-10.

[33] Ashish Vaswani, Noam Shazeer, Niki Parmar, Jakob Uszkoreit, Llion Jones, Aidan N Gomez, Łukasz Kaiser, and Illia Polosukhin. Attention is all you need. *Advances in Neural Information Processing Systems (NIPS)*, 30, 2017.

[34] Gui Xue, Adam R Aron, and Russell A Poldrack. Common neural substrates for inhibition of spoken and manual responses. *Cerebral Cortex*, 18(8):1923–1932, 2008.

[35] Adam R Aron, Tim E Behrens, Steve Smith, Michael J Frank, and Russell A Poldrack. Triangulating a cognitive control network using diffusion-weighted magnetic resonance imaging (mri) and functional mri. *Journal of Neuroscience*, 27(14):3743–3752, 2007.

[36] Tom M Mitchell, Svetlana V Shinkareva, Andrew Carlson, Kai-Min Chang, Vicente L Malave, Robert A Mason, and Marcel Adam Just. Predicting human brain activity associated with the meanings of nouns. *Science*, 320(5880):1191–1195, 2008.

[37] AM Clare Kelly, Lucina Q Uddin, Bharat B Biswal, F Xavier Castellanos, and Michael P Milham. Competition between functional brain networks mediates behavioral variability. *NeuroImage*, 39(1):527–537, 2008.

[38] Johan D Carlin and Nikolaus Kriegeskorte. Adjudicating between face-coding models with individual-face fmri responses. *PLoS Computational Biology*, 13(7):e1005604, 2017.

[39] Maria Geraldine Veldhuizen, Richard Keith Babbs, Barkha Patel, Wambura Fobbs, Nils B Kroemer, Elizabeth Garcia, Martin R Yeomans, and Dana M Small. Integration of sweet taste and metabolism determines carbohydrate reward. *Current Biology*, 27(16):2476–2485, 2017.

[40] Michael Hanke, Florian J Baumgartner, Pierre Ibe, Falko R Kaule, Stefan Pollmann, Oliver Speck, Wolf Zinke, and Jörg Stadler. A high-resolution 7-tesla fmri dataset from complex natural stimulation with an audio movie. *Scientific Data*, 1, 2014.

[41] Alex J Smola and Bernhard Schölkopf. A tutorial on support vector regression. *Statistics and Computing*, 14(3):199–222, 2004.

[42] Diederik P Kingma and Jimmy Ba. Adam: A method for stochastic optimization. In *International Conference on Learning Representations (ICLR)*, 2015.

NeurIPS Paper Checklist

1. **Claims**

   Question: Do the main claims made in the abstract and introduction accurately reflect the paper's contributions and scope?

   Answer: [Yes]

   Justification: The main claims in the abstract and introduction accurately reflect the paper's contributions, including the proposed OCL framework and its application to multi-subject and multi-site fMRI analyses.

   Guidelines:

   - The answer NA means that the abstract and introduction do not include the claims made in the paper.
   - The abstract and/or introduction should clearly state the claims made, including the contributions made in the paper and important assumptions and limitations. A No or NA answer to this question will not be perceived well by the reviewers.
   - The claims made should match theoretical and experimental results, and reflect how much the results can be expected to generalize to other settings.
   - It is fine to include aspirational goals as motivation as long as it is clear that these goals are not attained by the paper.

2. **Limitations**

   Question: Does the paper discuss the limitations of the work performed by the authors?

   Answer: [Yes]

   Justification: We discuss our primary assumptions in the Experiments section, and address the limitations and future directions of the proposed method in the Conclusion and Broader Impacts sections.

   Guidelines:

   - The answer NA means that the paper has no limitation while the answer No means that the paper has limitations, but those are not discussed in the paper.
   - The authors are encouraged to create a separate "Limitations" section in their paper.
   - The paper should point out any strong assumptions and how robust the results are to violations of these assumptions (e.g., independence assumptions, noiseless settings, model well-specification, asymptotic approximations only holding locally). The authors should reflect on how these assumptions might be violated in practice and what the implications would be.
   - The authors should reflect on the scope of the claims made, e.g., if the approach was only tested on a few datasets or with a few runs. In general, empirical results often depend on implicit assumptions, which should be articulated.
   - The authors should reflect on the factors that influence the performance of the approach. For example, a facial recognition algorithm may perform poorly when image resolution is low or images are taken in low lighting. Or a speech-to-text system might not be used reliably to provide closed captions for online lectures because it fails to handle technical jargon.
   - The authors should discuss the computational efficiency of the proposed algorithms and how they scale with dataset size.
   - If applicable, the authors should discuss possible limitations of their approach to address problems of privacy and fairness.
   - While the authors might fear that complete honesty about limitations might be used by reviewers as grounds for rejection, a worse outcome might be that reviewers discover limitations that aren't acknowledged in the paper. The authors should use their best judgment and recognize that individual actions in favor of transparency play an important role in developing norms that preserve the integrity of the community. Reviewers will be specifically instructed to not penalize honesty concerning limitations.

3. **Theory assumptions and proofs**

Question: For each theoretical result, does the paper provide the full set of assumptions and a complete (and correct) proof?

Answer: [Yes]

Justification: We provide the full set of assumptions in the Experiments section and include all proofs in the supplementary material.

Guidelines:

- The answer NA means that the paper does not include theoretical results.
- All the theorems, formulas, and proofs in the paper should be numbered and cross-referenced.
- All assumptions should be clearly stated or referenced in the statement of any theorems.
- The proofs can either appear in the main paper or the supplemental material, but if they appear in the supplemental material, the authors are encouraged to provide a short proof sketch to provide intuition.
- Inversely, any informal proof provided in the core of the paper should be complemented by formal proofs provided in appendix or supplemental material.
- Theorems and Lemmas that the proof relies upon should be properly referenced.

4. **Experimental result reproducibility**

Question: Does the paper fully disclose all the information needed to reproduce the main experimental results of the paper to the extent that it affects the main claims and/or conclusions of the paper (regardless of whether the code and data are provided or not)?

Answer: [Yes]

Justification: We provide all necessary details to reproduce the main experimental results in the Experiments section.

Guidelines:

- The answer NA means that the paper does not include experiments.
- If the paper includes experiments, a No answer to this question will not be perceived well by the reviewers: Making the paper reproducible is important, regardless of whether the code and data are provided or not.
- If the contribution is a dataset and/or model, the authors should describe the steps taken to make their results reproducible or verifiable.
- Depending on the contribution, reproducibility can be accomplished in various ways. For example, if the contribution is a novel architecture, describing the architecture fully might suffice, or if the contribution is a specific model and empirical evaluation, it may be necessary to either make it possible for others to replicate the model with the same dataset, or provide access to the model. In general. releasing code and data is often one good way to accomplish this, but reproducibility can also be provided via detailed instructions for how to replicate the results, access to a hosted model (e.g., in the case of a large language model), releasing of a model checkpoint, or other means that are appropriate to the research performed.
- While NeurIPS does not require releasing code, the conference does require all submissions to provide some reasonable avenue for reproducibility, which may depend on the nature of the contribution. For example
  (a) If the contribution is primarily a new algorithm, the paper should make it clear how to reproduce that algorithm.
  (b) If the contribution is primarily a new model architecture, the paper should describe the architecture clearly and fully.
  (c) If the contribution is a new model (e.g., a large language model), then there should either be a way to access this model for reproducing the results or a way to reproduce the model (e.g., with an open-source dataset or instructions for how to construct the dataset).
  (d) We recognize that reproducibility may be tricky in some cases, in which case authors are welcome to describe the particular way they provide for reproducibility. In the case of closed-source models, it may be that access to the model is limited in some way (e.g., to registered users), but it should be possible for other researchers to have some path to reproducing or verifying the results.

5. **Open access to data and code**

   Question: Does the paper provide open access to the data and code, with sufficient instructions to faithfully reproduce the main experimental results, as described in supplemental material?

   Answer: [Yes]

   Justification: The paper uses publicly available datasets for all empirical evaluations, and we will release the proposed method as part of our open-source toolkit for direct use in fMRI analysis.

   Guidelines:

   - The answer NA means that paper does not include experiments requiring code.
   - Please see the NeurIPS code and data submission guidelines (`https://nips.cc/public/guides/CodeSubmissionPolicy`) for more details.
   - While we encourage the release of code and data, we understand that this might not be possible, so "No" is an acceptable answer. Papers cannot be rejected simply for not including code, unless this is central to the contribution (e.g., for a new open-source benchmark).
   - The instructions should contain the exact command and environment needed to run to reproduce the results. See the NeurIPS code and data submission guidelines (`https://nips.cc/public/guides/CodeSubmissionPolicy`) for more details.
   - The authors should provide instructions on data access and preparation, including how to access the raw data, preprocessed data, intermediate data, and generated data, etc.
   - The authors should provide scripts to reproduce all experimental results for the new proposed method and baselines. If only a subset of experiments are reproducible, they should state which ones are omitted from the script and why.
   - At submission time, to preserve anonymity, the authors should release anonymized versions (if applicable).
   - Providing as much information as possible in supplemental material (appended to the paper) is recommended, but including URLs to data and code is permitted.

6. **Experimental setting/details**

   Question: Does the paper specify all the training and test details (e.g., data splits, hyperparameters, how they were chosen, type of optimizer, etc.) necessary to understand the results?

   Answer: [Yes]

   Justification: All training and testing details are clearly specified in the Experiments section.

   Guidelines:

   - The answer NA means that the paper does not include experiments.
   - The experimental setting should be presented in the core of the paper to a level of detail that is necessary to appreciate the results and make sense of them.
   - The full details can be provided either with the code, in appendix, or as supplemental material.

7. **Experiment statistical significance**

   Question: Does the paper report error bars suitably and correctly defined or other appropriate information about the statistical significance of the experiments?

   Answer: [Yes]

   Justification: We report error bars appropriately, define them clearly, and provide relevant information on statistical significance in the Experiments section.

   Guidelines:

   - The answer NA means that the paper does not include experiments.
   - The authors should answer "Yes" if the results are accompanied by error bars, confidence intervals, or statistical significance tests, at least for the experiments that support the main claims of the paper.

- The factors of variability that the error bars are capturing should be clearly stated (for example, train/test split, initialization, random drawing of some parameter, or overall run with given experimental conditions).
- The method for calculating the error bars should be explained (closed form formula, call to a library function, bootstrap, etc.)
- The assumptions made should be given (e.g., Normally distributed errors).
- It should be clear whether the error bar is the standard deviation or the standard error of the mean.
- It is OK to report 1-sigma error bars, but one should state it. The authors should preferably report a 2-sigma error bar than state that they have a 96% CI, if the hypothesis of Normality of errors is not verified.
- For asymmetric distributions, the authors should be careful not to show in tables or figures symmetric error bars that would yield results that are out of range (e.g. negative error rates).
- If error bars are reported in tables or plots, The authors should explain in the text how they were calculated and reference the corresponding figures or tables in the text.

8. **Experiments compute resources**

   Question: For each experiment, does the paper provide sufficient information on the computer resources (type of compute workers, memory, time of execution) needed to reproduce the experiments?

   Answer: [Yes]

   Justification: We provide detailed information about the computational resources used in the Experiments section.

   Guidelines:

   - The answer NA means that the paper does not include experiments.
   - The paper should indicate the type of compute workers CPU or GPU, internal cluster, or cloud provider, including relevant memory and storage.
   - The paper should provide the amount of compute required for each of the individual experimental runs as well as estimate the total compute.
   - The paper should disclose whether the full research project required more compute than the experiments reported in the paper (e.g., preliminary or failed experiments that didn't make it into the paper).

9. **Code of ethics**

   Question: Does the research conducted in the paper conform, in every respect, with the NeurIPS Code of Ethics `https://neurips.cc/public/EthicsGuidelines`?

   Answer: [Yes] .

   Justification: The research presented in this paper conforms to the NeurIPS Code of Ethics in all respects.

   Guidelines:

   - The answer NA means that the authors have not reviewed the NeurIPS Code of Ethics.
   - If the authors answer No, they should explain the special circumstances that require a deviation from the Code of Ethics.
   - The authors should make sure to preserve anonymity (e.g., if there is a special consideration due to laws or regulations in their jurisdiction).

10. **Broader impacts**

    Question: Does the paper discuss both potential positive societal impacts and negative societal impacts of the work performed?

    Answer: [Yes]

    Justification: Please refer to the Broader Impacts section.

    Guidelines:

    - The answer NA means that there is no societal impact of the work performed.

- If the authors answer NA or No, they should explain why their work has no societal impact or why the paper does not address societal impact.
- Examples of negative societal impacts include potential malicious or unintended uses (e.g., disinformation, generating fake profiles, surveillance), fairness considerations (e.g., deployment of technologies that could make decisions that unfairly impact specific groups), privacy considerations, and security considerations.
- The conference expects that many papers will be foundational research and not tied to particular applications, let alone deployments. However, if there is a direct path to any negative applications, the authors should point it out. For example, it is legitimate to point out that an improvement in the quality of generative models could be used to generate deepfakes for disinformation. On the other hand, it is not needed to point out that a generic algorithm for optimizing neural networks could enable people to train models that generate Deepfakes faster.
- The authors should consider possible harms that could arise when the technology is being used as intended and functioning correctly, harms that could arise when the technology is being used as intended but gives incorrect results, and harms following from (intentional or unintentional) misuse of the technology.
- If there are negative societal impacts, the authors could also discuss possible mitigation strategies (e.g., gated release of models, providing defenses in addition to attacks, mechanisms for monitoring misuse, mechanisms to monitor how a system learns from feedback over time, improving the efficiency and accessibility of ML).

11. **Safeguards**

    Question: Does the paper describe safeguards that have been put in place for responsible release of data or models that have a high risk for misuse (e.g., pretrained language models, image generators, or scraped datasets)?

    Answer: [NA] .

    Justification: This paper does not utilize pretrained language models, image generators, or datasets obtained through web scraping.

    Guidelines:

    - The answer NA means that the paper poses no such risks.
    - Released models that have a high risk for misuse or dual-use should be released with necessary safeguards to allow for controlled use of the model, for example by requiring that users adhere to usage guidelines or restrictions to access the model or implementing safety filters.
    - Datasets that have been scraped from the Internet could pose safety risks. The authors should describe how they avoided releasing unsafe images.
    - We recognize that providing effective safeguards is challenging, and many papers do not require this, but we encourage authors to take this into account and make a best faith effort.

12. **Licenses for existing assets**

    Question: Are the creators or original owners of assets (e.g., code, data, models), used in the paper, properly credited and are the license and terms of use explicitly mentioned and properly respected?

    Answer: [NA]

    Justification: This paper does not use existing assets

    Guidelines:

    - The answer NA means that the paper does not use existing assets.
    - The authors should cite the original paper that produced the code package or dataset.
    - The authors should state which version of the asset is used and, if possible, include a URL.
    - The name of the license (e.g., CC-BY 4.0) should be included for each asset.
    - For scraped data from a particular source (e.g., website), the copyright and terms of service of that source should be provided.

- If assets are released, the license, copyright information, and terms of use in the package should be provided. For popular datasets, `paperswithcode.com/datasets` has curated licenses for some datasets. Their licensing guide can help determine the license of a dataset.
- For existing datasets that are re-packaged, both the original license and the license of the derived asset (if it has changed) should be provided.
- If this information is not available online, the authors are encouraged to reach out to the asset's creators.

13. **New assets**

    Question: Are new assets introduced in the paper well documented and is the documentation provided alongside the assets?

    Answer: [NA]

    Justification: This paper does not release new assets

    Guidelines:

    - The answer NA means that the paper does not release new assets.
    - Researchers should communicate the details of the dataset/code/model as part of their submissions via structured templates. This includes details about training, license, limitations, etc.
    - The paper should discuss whether and how consent was obtained from people whose asset is used.
    - At submission time, remember to anonymize your assets (if applicable). You can either create an anonymized URL or include an anonymized zip file.

14. **Crowdsourcing and research with human subjects**

    Question: For crowdsourcing experiments and research with human subjects, does the paper include the full text of instructions given to participants and screenshots, if applicable, as well as details about compensation (if any)?

    Answer: [NA]

    Justification: This paper does not involve crowdsourcing nor direct research with human subjects.

    Guidelines:

    - The answer NA means that the paper does not involve crowdsourcing nor research with human subjects.
    - Including this information in the supplemental material is fine, but if the main contribution of the paper involves human subjects, then as much detail as possible should be included in the main paper.
    - According to the NeurIPS Code of Ethics, workers involved in data collection, curation, or other labor should be paid at least the minimum wage in the country of the data collector.

15. **Institutional review board (IRB) approvals or equivalent for research with human subjects**

    Question: Does the paper describe potential risks incurred by study participants, whether such risks were disclosed to the subjects, and whether Institutional Review Board (IRB) approvals (or an equivalent approval/review based on the requirements of your country or institution) were obtained?

    Answer: [NA]

    Justification: This paper does not involve crowdsourcing nor direct research with human subjects.

    Guidelines:

    - The answer NA means that the paper does not involve crowdsourcing nor research with human subjects.

- Depending on the country in which research is conducted, IRB approval (or equivalent) may be required for any human subjects research. If you obtained IRB approval, you should clearly state this in the paper.
- We recognize that the procedures for this may vary significantly between institutions and locations, and we expect authors to adhere to the NeurIPS Code of Ethics and the guidelines for their institution.
- For initial submissions, do not include any information that would break anonymity (if applicable), such as the institution conducting the review.

16. **Declaration of LLM usage**

    Question: Does the paper describe the usage of LLMs if it is an important, original, or non-standard component of the core methods in this research? Note that if the LLM is used only for writing, editing, or formatting purposes and does not impact the core methodology, scientific rigorousness, or originality of the research, declaration is not required.

    Answer: [NA]

    Justification: We used large language models solely for writing assistance, editing, and formatting purposes.

    Guidelines:

    - The answer NA means that the core method development in this research does not involve LLMs as any important, original, or non-standard components.
    - Please refer to our LLM policy (`https://neurips.cc/Conferences/2025/LLM`) for what should or should not be described.